Low Temperature Crystal Structure Behaviour of Complex Yttrium Aluminium Oxides $YAlO_3$ and $Y_3Al_5O_{12}$

A. Senyshyn[a,*] and L. Vasylechko[b]

[a]Forschungs-Neutronenequelle Heinz Maier-Leibnitz FRM-II, Technische Universität München
Lichtenbergstrasse 1, D-85748 Garching b. München, Germany
[b]Lviv Polytechnic National University, 12 Bandera Str, 79013 Lviv, Ukraine

Crystal structures of two yttrium aluminium oxides, namely $YAlO_3$ and $Y_3Al_5O_{12}$, were investigated in the temperature range 3.4–300 K by high-resolution neutron powder diffraction. Neither traces of phase transformations nor discontinuous changes of physical properties were observed. Thermal expansion of yttrium aluminium oxides was evaluated in terms of 1st order Grüneisen approximation, where the Debye temperatures and the Grüneisen parameters have been estimated for both compositions. Anomalies in the thermal expansion of yttrium aluminium perovskite have been observed and modelled using the Einstein oscillator with negative Grüneisen parameter. Extended bond length analysis revealed significant thermally-driven modifications of the aluminium–oxygen framework.

1. Introduction

Yttrium aluminium perovskite $YAlO_3$ (YAP) and yttrium aluminium garnet $Y_3Al_5O_{12}$ (YAG) are extensively studied during the last five decades due to their great technological relevance, where their use as host materials in solid-state lasers of different kinds [1–9] is the most widespread areas of application for both compounds. Since the discovery of YAG:Nd laser in 1964 [1], the Nd doped $Y_3Al_5O_{12}$ remains one of the most popular laser materials and the large single crystals are grown on a commercial base. The Yb-doped $Y_3Al_5O_{12}$ is considered as prospective materials for cryogenically cooled (80–100 K) solid-state lasers, which promise a revolution in power scalability while maintaining a good beam quality [7–9]. Single crystals of yttrium aluminium perovskite $YAlO_3$, doped with Nd, Tm, Er and Ho are also well known as active and passive laser media [2–5, 10, 11]. YAP doped with Yb^{2+} or V^{4+} was proposed as material for tunable solid-state lasers [12, 13], whereas optical properties of $YAlO_3$:Mn crystals are suitable for holographic and optical storage devices [14]. Besides the laser applications, both materials are used as phosphors and scintillators of α- and β-radiation, cathodoluminescence screens, and X-ray imaging screens [15–17]. Variously doped YAG materials have been proposed as optical pressure sensors up to very high pressure (*ca.* 180 GPa) [18]. Single crystalline substrates of $YAlO_3$ are used for the epitaxy of thin films of HTSC [19, 20], manganites with colossal magnetoresistive effect [21] and $TbMnO_3$ multiferroic films [22]. Jourdan et al. [23] reported on the epitaxial growth of the heavy fermion superconductor UNi_2Al_3 on the (112)-oriented $YAlO_3$ substrates.

Practical applications of $Y_3Al_5O_{12}$ and $YAlO_3$ as laser matrices and substrate materials for thin films epitaxy make thermal behaviour issue of crystal structures in a wide temperature range a relevant task. In particular, coefficient of thermal expansion (TEC, α) is one of the key thermo-optical properties of cryogenically cooled solid-state lasers, along with thermal conductivity and thermal coefficient of refractive index [7, 8]. Consequently, first examination of thermal expansion of $Y_3Al_5O_{12}$ [24–26] appears in 1970, shortly after first publications on YAG:Nd laser performance. Since then a lot of reports on TEC determination in nominally pure and doped YAG by various experimental techniques have been published (see, for example Refs. [7–9, 27] and references herein). According to the literature, the value of TEC of YAG at room temperature (RT) varies from 6.1×10^{-6} to 7.3×10^{-6} K^{-1}. Low-temperature (77–300 K) and high-temperature (303–1073 K) dependences of the TEC of pure and doped YAG crystals were reported in Refs. [7, 8, 27] and [28], respectively. Recently, lattice dynamics and first principle simulations have been applied for a calculation of TEC in $Y_3Al_5O_{12}$ as a function of pressure and temperature up to 1500 (1600 K) [29, 30]. However, all these publications are limited mainly to the study of the lattice expansion and thermal expansion coefficient. To our best knowledge, there is no information in the literature on the detailed investigation of the thermal behaviour of the principal structural parameters of $Y_3Al_5O_{12}$ such as interatomic distances and angles, atomic displacement parameters, etc.

Study of the thermal behaviour of $YAlO_3$ perovskite structure starts in 1972 by using holographic interferometry for the measurement of the thermal expansion coefficients of YAG:Nd and YAP:Nd crystals [31]. The high-temperature behaviour of the pure and variously doped $YAlO_3$ have been studied *in situ* applying neutron [32], X-ray [33] and X-ray synchrotron [34] powder

---

*corresponding author; e-mail: Anatoliy.Senyshyn@frm2.tum.de

diffraction techniques. It was shown that $YAlO_3$ reveals a strong anisotropy of thermal expansion in different crystallographic directions. The anisotropy of thermal expansion of $YAlO_3$ was confirmed by recent investigations of high-temperature thermal behaviour of TEC of Tm- and Ho-doped YAP crystals performed in [35, 36]. Low-temperature examinations of structural behaviour of $YAlO_3$ performed *in situ* by using neutron and X-ray synchrotron powder diffraction techniques revealed pronounced anomalies in *b*-direction, which occur in both Mn and Nd-doped crystals [34].

In the present manuscript we report the results of thorough examination of low-temperature behaviour of yttrium aluminium garnet $Y_3Al_5O_{12}$ and yttrium aluminium perovskite $YAlO_3$ — two most important technological crystals in the rich family of group III metal-aluminium oxides.

2. Experimental

Single crystals of YAG and YAP:Nd were grown by the Czochralski method in Scientific Research Company "Carat" (Lviv, Ukraine) [37]. The YAP:Nd crystals were pulled in the [010] direction in *Pbnm* setting. For crystal growth experiments, a stoichiometric mixture made of pure Y_2O_3 and Al_2O_3 (99.99 w/w% of main components) was used. The Nd_2O_3 dopant was introduced directly into the crucible before charge melting in 1 w/w% amount. Constant temperature gradients in the growth direction as well as a flat solid–liquid interface during growth process have been ensured with a special design of the heat-insulating unit [37].

For powder diffraction studies a part of the single crystalline ingot was crushed, ground using corundum mill and homogenized in size. Short check with X-ray powder diffraction reveals only the Bragg reflections consistent with $GdFeO_3$ type of structure for $YAlO_3$ and $Al_2Ca_3Si_3O_{12}$ structure type for $Y_3Al_5O_{12}$. Elastic coherent neutron scattering experiments were performed on the high-resolution powder diffractometer SPODI at the research reactor FRM-II (Garching, Germany) [38]. Monochromatic neutrons ($\lambda = 1.5482$ Å) were obtained at a 155° take-off angle using the (551) reflection of a vertically-focused composite Ge monochromator. The vertical position-sensitive multidetector (300 mm effective height) consisting of 80 ^{3}He tubes and covering an angular range of 160 deg 2θ was used for data collection. Measurements were performed in the Debye–Scherrer geometry. The powder sample (*ca.* 2 cm^3 in volume) was filled into a thin-wall (0.15 mm) vanadium can of 13 mm in diameter and then mounted in the top-loading closed-cycle refrigerator. Helium 4.6 was used as a heat transmitter. The instantaneous temperature was measured using two thin film resistance cryogenic temperature sensors Cernox and controlled by a temperature controller from LakeShore^{TM}. Two dimensional powder diffraction data were collected at fixed temperatures in the range of 3.4–300 K upon heating and then corrected for geometrical abberations and curvature of the Debye–Scherrer rings as described in Ref. [38].

Treatment of powder diffraction data was carried out using the Rietveld technique implemented into the software package FullProf [39]. The peak profile shape was described by a pseudo-Voigt function. The background of the diffraction pattern was fitted using a linear interpolation between selected data points in non-overlapping regions. The scale factor, lattice parameter, fractional coordinates of atoms and their isotropic displacement parameters (the anisotropic displacement parameters were refined for $Y_3Al_5O_{12}$ case), zero angular shift, profile shape parameters, and half width (Caglioti) parameters were allowed to vary during the fitting.

3. Results and discussion

In contrast to observations from the X-ray powder diffraction indicating the structural purity of the obtained materials, the high-resolution neutron powder diffraction revealed some weak traces of corundum present, which were further confirmed by X-ray examination on neutron irradiated samples. After numerous cross checks the traces of corundum have been attributed to the contaminations from the milling materials (and not to residue amount of Al_2O_3 used for crystal growth) and have been included as an independent phase to the Rietveld refinement model.

3.1. Yttrium aluminium garnet

The best Rietveld fit to the powder diffraction pattern collected at 3.4 K was obtained with parameters listed in Table and the graphical representation of the Rietveld refinement is shown in Fig. 1, accordingly. Thermal evolution of $Y_3Al_5O_{12}$ lattice parameters is shown in Fig. 2a, where cell dimensions smoothly and nonlinearly grow on heating. The lattice of $Y_3Al_5O_{12}$ is characterized by a very weak structural response on temperature, i.e. temperature difference of *ca.* 300 K results in the increase of lattice parameter by 0.0118 Å (about 0.1%), which correspond to a linear thermal expansion coefficient of $6.4(5) \times 10^{-6}$ K^{-1} at room temperature (calculated as $\alpha_l(T) = \mathrm{d}\ln l(T)/\mathrm{d}T$).
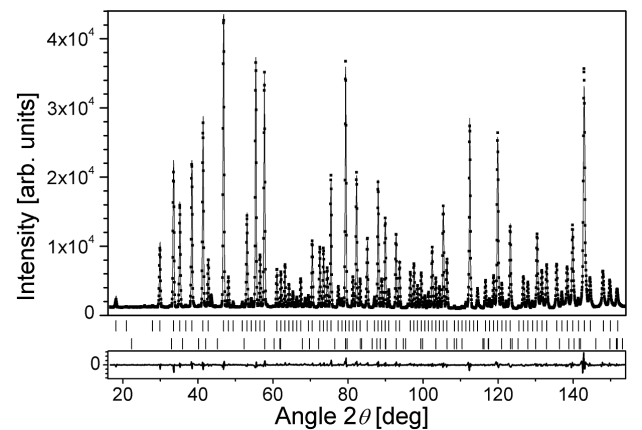
Fig. 1. Results of Rietveld refinements of neutron powder diffraction data for $Y_3Al_5O_{12}$ at 3.4 K.

Experimental structural parameters of $Y_3Al_5O_{12}$ and $YAlO_3$ at $T = 3.4$ K. Numbers in parentheses give statistical deviations in the last significant digits.   TABLE

Atom site	Wyckoff symbol	x/a [frac. un.]	y/b [frac. un.]	z/c [frac. un.]	u_{iso} [Å²]	u_{11} [Å²]	u_{22} [Å²]	u_{33} [Å²]	u_{12} [Å²]	u_{13} [Å²]	u_{23} [Å²]
$Y_3Al_5O_{12}$, space group $Ia\text{-}3d$ (No. 230), $a = 11.99954(17)$ Å											
Y1	24c	1/8	0	1/4	0.0047(3)	0.0059(4)	0.0041(2)	u_{22}	0	0	0.0002(3)
Al1	16a	0	0	0	0.0043(3)	0.0043(3)	u_{11}	u_{11}	−0.0005(6)	u_{12}	u_{12}
Al2	24d	3/8	0	1/4	0.0039(6)	0.0025(9)	0.0045(5)	u_{22}	0	0	0
O1	96h	−0.03070(4)	0.05088(5)	0.14895(5)	0.0053(3)	0.0059(3)	0.0062(3)	0.0039(3)	0.0009(2)	0.00006(19)	0.0013(2)
Fit residuals: $R_{\mathrm{p}} = 4.30\%$, $R_{\mathrm{wp}} = 5.81\%$, $R_{\mathrm{exp}} = 1.76\%$, $\chi^2 = 10.9$											
$YAlO_3$, space group $Pbnm$ (No. 62), $a = 5.17242(9)$ Å, $b = 5.32659(9)$ Å, $c = 7.36085(13)$ Å											
Y1	4c	0.01241(12)	0.55406(9)	1/4	0.00150(13)	–	–	–	–	–	–
Al1	4a	0	0	0	0.0016(2)	–	–	–	–	–	–
O1	4c	−0.08385(15)	−0.0220(1)	1/4	0.00070(16)	–	–	–	–	–	–
O2	8d	0.2047(1)	0.29483(9)	0.04427(7)	0.00177(13)	–	–	–	–	–	–
Fit residuals: $R_{\mathrm{p}} = 3.21\%$, $R_{\mathrm{wp}} = 4.08\%$, $R_{\mathrm{exp}} = 1.30$, $\chi^2 = 9.88$											

As it has been shown in numerous works [40–42] the obtained thermal dependences of lattice parameters can be modelled in the frame of the first order Grüneisen approximation

$$V(T) = V_0 + \frac{\gamma}{K_{\mathrm{T}}} U(T)$$

$$= V_0 + \frac{\gamma}{K_{\mathrm{T}}} \left[9Nk_{\mathrm{B}}T \left(\frac{T}{\theta_{\mathrm{D}}}\right)^3 \int_0^{\theta_{\mathrm{D}}/T} \frac{x^3}{\mathrm{e}^x - 1}\,\mathrm{d}x \right], \quad (1)$$

where V_0 denotes the hypothetical cell volume at zero temperature, γ is the Grüneisen constant, K_{T} is the bulk modulus, and U is the internal energy of the system. Both γ and K_{T} are assumed to be temperature independent. The use of the Debye approximation for the internal energy U in Eq. (1) with characteristic temperature θ_{D} provides a reasonable description.

The least-square minimization fit of experimental temperature dependence of cell volumes by Eq. (1) yields $1727.8(1)$ Å³, $618 \times 10^{-14} \pm 108 \times 10^{-14}$ Pa^{-1} and 534 ± 112 K for V_0, γ/K_{T} ratio and θ_{D}, respectively. The fit was characterized by a high coefficient of determination 0.99939 and the graphical results are shown in Fig. 2a by dashed lines. The first-order Grüneisen approximation delivers γ/K_{T} ratio and the determination of the Grüneisen constant requires the knowledge of bulk modulus, which has been determined for $Y_3Al_5O_{12}$ by Hofmeister and Campbell [43] from measured infrared vibrational frequencies ($K_{\mathrm{T}} = 220$ GPa), by Stoddart et al. [44] and by Alton and Barow [45] using a combination of the Brillouin scattering and refractive index measurements ($K_{\mathrm{T}} = 189$ GPa and 185.2 GPa, respectively), by Xu and Ching [46] using first-principles local-density calculations ($K_{\mathrm{T}} = 221.1$–228.6 GPa). Approximately 17% uncertainty in the value of γ/K_{T} ratio along with 10% discrepancy for literature values of bulk modulus define the Grüneisen constant in the range 0.95–1.66, indicating weak anharmonicity of the lattice vibrations and, as a consequence, relatively low thermal expansivity. Low lattice expansion seems to be quite typical for materials with garnet structure [47], where bond-length thermal

elongation is compensated by the tilting and distortion of the coordination polyhedra.
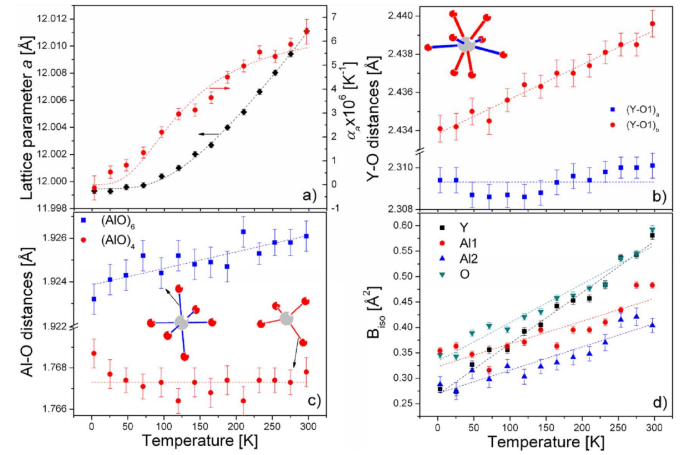
Fig. 2. Thermal dependence of lattice parameter and thermal expansion coefficient in $Y_3Al_5O_{12}$ (a); evolution of Y–O (b) and Al–O (c) interatomic distances and isotropic displacement parameters (d). Lines in (a) correspond to the modelling using Eq. (1) and lines in (b)–(d) denote linear fits and are shown as guides for the eyes.

Three types of the vortex-shared cation coordination polyhedra are forming the $Y_3Al_5O_{12}$ structure, namely YO_8, AlO_4, and AlO_6. The yttrium–oxygen coordination polyhedron in $Y_3Al_5O_{12}$ has a form of distorted cube, which is built on two distinct yttrium–oxygen distances undergoing different thermal behaviour (Fig. 2b). The shorter Y–O interatomic distance (Y–O1)$_a$ remains nearly independent on temperature in the whole range investigated, whereas the longer one (Y–O1)$_b$ increases linearly upon heating.

The metal cations in regular octahedral (AlO_6) and tetrahedral (AlO_4) coordination are yet another structural feature of garnets. Thermal dependences of Al–O interatomic distances display different character

(Fig. 2c). The intraoctahedral Al–O distances weakly increase on heating, whereas the tetrahedral one remains nearly temperature-independent (or even showing some tendency to contract with increasing temperatures). Such thermal rigidity often occurs in tetrahedral oxygen coordinations [48] and on the first glance it can be attributed to the increase of the covalent part in the tetrahedral bonding leading to shorter Al–O bond length etc. Hence, performed bond valence calculations revealed 3.125(2), 2.636(2), 2.686(2), −1.892(1) bond valence sums for Y, Al1, Al2 and O sites at 3.4 K, respectively, indicating similar type of Al–O bonding for both Al1 and Al2. On the other hand, the bond valence calculations already utilize R_0 values adapted to special coordinations and so forth. This general problem is not trivial and more light on it can be shed by careful and especially dedicated theoretical research, which is beyond the scope of the current contribution and, therefore, will not be considered here in detail.

The isotropic displacement parameters for structural sites of $Y_3Al_5O_{12}$ are shown in Fig. 2d. At 3.5 K the $u_{iso}(Al2) \approx u_{iso}(O) > u_{iso}(Y) \approx u_{iso}(Al1)$ have been found and the heating up to room temperature leads to an increase of u_{iso} for all constituents with the slope fulfilling the relationship $u_{iso}(Y) > u_{iso}(O) > u_{iso}(Al1) \approx u_{iso}(Al2)$. Assuming the root mean square displacement to be proportional to the mass of constituent the observed behaviour can be attributed to a little static disorder on the Al2 site along with temperature-driven disorder of Y inside the distorted cubic coordination. Analysis of components of the anisotropic displacement tensor indicated that the orientation of principal axes of the ellipsoid remain nearly constant within the limits of uncertainties and the axes components smoothly increase upon heating with $u_{11}(Y) > u_{22}(Y) = u_{33}(Y)$, $u_{11}(Al1) = u_{22}(Al1) = u_{33}(Al1)$, $u_{11}(Al2) < u_{22}(Al2) = u_{33}(Al2)$ and $u_{11}(O) \approx u_{22}(O) > u_{33}(O)$.

3.2. Yttrium aluminium perovskite

Graphical result of the Rietveld refinement of neutron powder diffraction pattern for $YAlO_3$ collected at 3.5 K is shown in Fig. 3 and the best fit has been obtained with the parameters listed in Table. The data analysis revealed the $GdFeO_3$ type of structure in the whole temperature range considered, where structural parameters smoothly react on the temperature change. Similar to the rare-earth alluminates [34] thermal expansion of $YAlO_3$ has been found anisotropic, where lattice parameters a and c nonlinearly and smoothly increase upon heating and the lattice parameter b shows a well-pronounced minimum around 160 K. Thermal expansion coefficients in a and c directions of the orthorhombic lattice follow the nonlinear increasing trend and are very similar in magnitude, whereas the α_b coefficient possesses negative values in the temperature range 3.5–160 K with the minimum around 75 K. The observed negative thermal expansion in b-direction of $GdFeO_3$-type structure is not new. It has been already established for the series of perovskite-type rare-earth alluminates [34] and gallates [41, 49] and

has been attributed to the coupling of crystalline electric field (CEF) levels of $4f$ ions to the lattice and, consequently, was not expected to occur in $YAlO_3$. Despite its weakness, the possible reasons for this effect are unclear and require to be characterized explicitly.
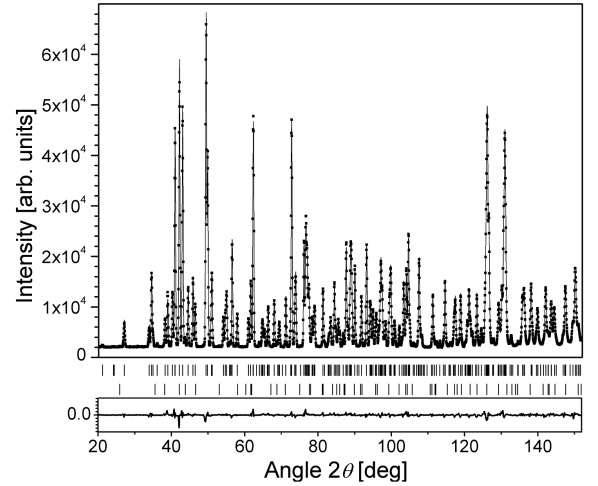
Fig. 3. Results of Rietveld refinements of neutron powder diffraction data for $YAlO_3$ at 3.4 K.

Recently, Fortes et al. [50] found that the lattice parameters (and not only the cell volume) of α-$MgSO_4$ can be fitted by a modified Eq. (1)

$$l(T) = l_0 + x_1 U_D(T), \qquad (2)$$

where l corresponds to lattice parameter, l_0 denotes its hypothetical value at zero temperature and x_1 is the fitting parameter (in the case of using cell volumes it becomes the meaning of the γ/K_T ratio). Therefore, fitting of obtained thermal dependences of a and c lattice parameters as well as cell volume has been performed using the protocol previously described for $Y_3Al_5O_{12}$. The best results (shown by lines) have been obtained with the parameters displayed in Figs. 4a–c. Beyond the meaningless x_1 values obtained from the temperature evolution of a and c lattice parameters the obtained Debye temperatures 466(91) K and 440(87) K were quite consistent and are in agreement with the θ_D from the nonlinear fit of cell volumes ($\theta_D = 545(134)$ K) as well as to the data from Ref. [51], where temperature-driven shifts of zero phonon lines (R lines) of $YAlO_3$ apparent at low temperature have been considered and the $\theta_D = 465 \pm 15$ K has been estimated. The γ/K_T ratio has been determined as $510(134) \times 10^{-14}$ Pa^{-1}, which using theoretical value of 188 GPa [52] and experimental one of 192(2) GPa [53] gives a spread for the Grüneisen parameter from 0.7 to 1.25. The observed range of values is in agreement with the Grüneisen parameter determined for $Y_3Al_5O_{12}$ and isostructural rare-earth containing perovskites [54–56].

As it has been shown in Ref. [50], Eq. (2) is not suitable for description of the negative thermal expansion occurring in the b-direction of the β-$MgSO_4$ lattice. Taking into account that the total thermal expansion coefficient,
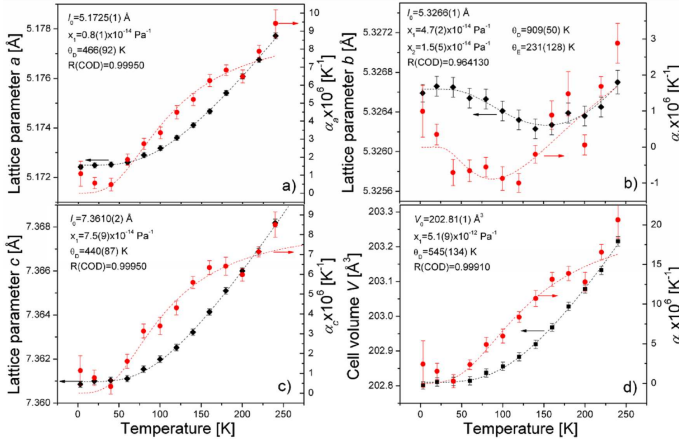
Fig. 4. Thermal dependence of the lattice parameters (a)–(c) and cell volume (d) of $YAlO_3$ as well as corresponding thermal expansion coefficients. Lines correspond to the modelling using Eq. (1)–(3).

similar to heat capacity, is an additive property, one more term, describing the lattice contraction, was introduced by Fortes et al. [50]:

$$l(T) = l_0 + x_1 U_D(T) + x_2 U_E(T)$$

$$= l_0 + x_1 U_D(T) + x_2 \left[\frac{3Nk_B\theta_E}{\exp(\theta_E/T) - 1} \right], \qquad (3)$$

where the x_2 fitting parameter is constrained as strictly negative, i.e. $x_2 < 0$, and corresponds to a negative Grüneisen parameter. It has also been proposed in Ref. [50] to use the Einstein model U_E as a single mode with fixed frequency (with negative mode Grüneisen parameter), corresponding to a fixed Einstein temperature θ_E. This approach was found successful in simulations of negative thermal expansion occurring in the b-direction of the β-$MgSO_4$ lattice [50], $Li_2B_4O_7$ [57] as well as in Pr-containing rare earth gallates [41, 49].

Similar to the observations from Ref. [41], the least-square fit of b lattice parameters by Eq. (3) yields much higher Debye temperature $\theta_D = 909(50)$ K in comparison to these obtained from the nonlinear fit of a, c lattice parameters and cell volume. This might be related to the limited temperature range considered, which along with the superposition of two effects results in overestimated θ_D for the b-direction of the orthorhombic lattice. The $\theta_E = 231(128)$ K was determined for $YAlO_3$, which is in line with values for $Pr(Nd)GaO_3$ pseudo-binary system [41]. Observed agreement might indicate a similarity in the nature for negative thermal expansion in yttrium aluminate and praseodymium-based gallates with perovskite structure and, consequently, requires an extended bond-length analysis.

In contrast to $Y_3Al_5O_{12}$, the nominal oxygen coordination number for yttrium in $YAlO_3$ is twelve and has a form of distorted cubooctahedron. It is built on eight distinct types of distances from yttrium to oxygens (O1 and O2), which range from 2.25 Å to 3.27 Å,

where Y–O2 distances appear twice. It makes overall 12 Y–O bonds and their temperature dependences are shown in Fig. 5a. Among twelve yttrium–oxygen distances the $(Y–O1)_3$, $(Y–O1)_2$ and $2 \times (Y–O2)_1$ are the longest one and do not entirely belong to the first coordination sphere of yttrium. This may cause a reduction of an effective coordination number for Y–O coordination polyhedron from 12 to 10, 9 or even eight. The genuine coordination number of A–O coordination polyhedron in ABX_3 perovskites was the matter of significant discussion in the past [34, 58–60] and still remains sometimes an issue. It can be determined by the analysis of coordination polyhedron and bond-length distortion, bond valence sums as well as analysis of thermally-induced bond-lengths elongation. The absolute elongation of yttrium–oxygen bonds shown in Fig. 5b (using the same colour scheme as in Fig. 5a), from which the thermally-driven contraction for $(Y–O1)_2$ and $2 \times (Y–O2)_1$ bonds is obvious. These selected longest interatomic distances do not take part in the thermal expansion, which might indicate an effective coordination number of 9 for yttrium–oxygen environment in $YAlO_3$.
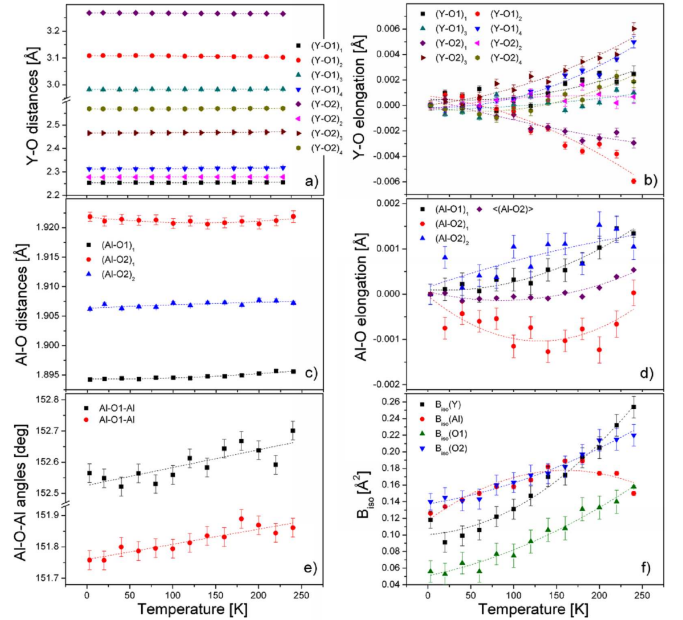
Fig. 5. Thermal evolution of Y–O (a) interatomic distances and their relative expansion (b), evolution of Al–O (c) interatomic distances and their relative expansion (d), thermal dependence of Al–O–Al interoctahedral angles (e), isotropic displacement parameters in $YAlO_3$ upon heating (f). Lines in (a)–(f) denote linear/polynomial fits and are shown as guides for the eyes.

The perovskite-structure for ABX_3 type compounds can also be presented as a framework of corner-shared BX_6 octahedra forming the primitive perovskite cell. In contrast to garnet and the ideal perovskite, the octahedral distortion is a typical feature in the $GdFeO_3$ type of structure. It reflects into three distinct types of

B–X (or specifically Al–O) distances, namely $(Al–O1)_1$, $(Al–O2)_1$, $(Al–O2)_2$, where each of them is doubly degenerated. In contrast to yttrium–oxygen coordination the spread of Al–O distances is much lower (1.894(2)–1.922(2) Å at 3.5 K). Thermal evolution of Al–O bond lengths is shown in Fig. 5c showing their low expansitivities. View of the absolute elongation of aluminium–oxygen bond lengths (Fig. 5d) indicated their different thermal behaviour: the $(Al–O1)_1$ and $(Al–O2)_2$ intraoctahedral distances increase in a similar way upon heating, whereas $(Al–O2)_1$ one shows some tendency for contraction. This effect makes the distorted AlO_6 octahedra in $YAlO_3$ stiffer to temperature changes as compared to these in $Y_3Al_5O_{12}$. Solely contraction tendency of one Al–O bond length is not enough to explain the negative thermal expansion in $GdFeO_3$-type perovskite. In Ref. [41] it has been shown that a distortional mechanism of lattice contraction may occur under decrease of mean $\langle B–X2 \rangle$ distance upon heating. Temperature dependence of $\langle Al–O2 \rangle$ distance shown in Fig. 5e displays nearly constant temperature behaviour, which along with the increase of Al–O2–Al interatomic angles (Fig. 5e) give neither clear evidence for rotational nor distortion mechanism of negative thermal expansion in $YAlO_3$. Taking into account an extremely small magnitude of the observed anomaly, its origin, most probably, cannot be resolved using diffraction methods as the current study was performed performed nearly on the verge of its accuracy.

The isotropic displacement parameters for Y, Al, O1 and O2 atomic sites are shown in Fig. 5f. Similar to $Y_3Al_5O_{12}$ the yttrium site shows the highest increase of u_{iso} upon heating, which might be related to the features in its coordination. The slope of $u_{iso}(T)$ curves for O1 and O2 sites has been found very similar, which is in agreement with the assumption about proportionality of the root mean square displacement and the mass of vibrating species. Again, similar to garnet (Al1 site), the aluminium site in $YAlO_3$ at 3.5 K possesses quite high isotropic displacement parameter (close to the value for O2). Contrary, upon heating the $u_{iso}(Al)$ displays nonlinear behaviour with a maximum around 160–180 K, which is correlating to the $\alpha_b = 0$ point.

4. Conclusions

The crystal structure of two complex yttrium aluminium oxides $Y_3Al_5O_{12}$ and $YAlO_3$ has been studied at low temperatures using high-resolution neutron powder diffraction. Structural features of both garnet and perovskite type materials have been compared in both qualitative and quantitative ways and an attempt to build structural pattern of consistence for tightly-related complex oxides has been made.

The $Y_3Al_5O_{12}$ responds on heating in normal way similar to most of inorganic compounds, whereas $YAlO_3$ displayed unexpected weak negative thermal expansion in the b-direction of its orthorhombic lattice, which rules out the previous assumption of a crystal electric field — phonon coupling nature of the negative thermal expansion in the series of perovskite type rare-earth gallates

and aluminates. This indicates that the softening of the low lying optical phonons, possibly originated from yttrium motion, might play a more crucial role in the anharmonicity as expected. Hence, due to the weakness of the anomalous thermal expansion, its origin and structural mechanism cannot be elucidated with enough confidence and requires further research.

Thermal dependences of lattice parameters were treated using first order Grüneisen approximation, where anomalous thermal expansion has been simulated using the Einstein oscillator with negative Grüneisen parameter. On the basis of that the Debye temperatures for both $Y_3Al_5O_{12}$ and $YAlO_3$ have been determined. Using literature data for bulk modules the Grüneisen parameters were estimated for both $Y_3Al_5O_{12}$ and $YAlO_3$.

References

[1] J.E. Geustic, H.M. Marcos, L.G. Van Uitert, *Appl. Phys. Lett.* **4**, 182 (1964).

[2] M.J. Weber, M. Bass, K. Andringa, *Appl. Phys. Lett.* **15**, 342 (1969).

[3] M. Bass, M.J. Weber, *Appl. Phys. Lett.* **17**, 395 (1970).

[4] G.A. Massey, *Appl. Phys. Lett.* **17**, 213 (1970).

[5] A.A. Kaminskii, *Physica Status Solidi A* **148**, 9 (1995).

[6] A. Ikesue, T. Kinoshita, K. Kamata, K. Yoshida, *J. Am. Ceram. Soc.* **78**, 1033 (1995).

[7] R.L. Aggarwal, D.J. Ripin, J.R. Ochoa, T.Y. Fan, *SPIE Proc.* **5707**, 165 (2005).

[8] T.Y. Fan, D.J. Ripin, R.L. Aggarwal, J.R. Ochoa, B. Chann, M. Tilleman, J. Spitzberg, *IEEE J. Sel. Top. Quant. Electron.* **13**, 448 (2007).

[9] J. Petit, B. Viana, Ph. Goldner, J.-P. Roger, D. Fournier, *J. Appl. Phys.* **108**, 123108 (2010).

[10] A.O. Matkovskii, D.I. Savytskii, D.Yu. Sugak, I.M. Solskii, L.O. Vasylechko, Ya.A. Zhydachevskii, M. Mond, K. Petermann, F. Wallrafen, *J. Cryst. Growth* **241**, 455 (2002).

[11] X.M. Duan, B.Q. Yao, G. Li, T.H. Wang, X.T. Yang, Y.Z. Wang, G.J. Zhao, Q. Dong, *Laser Phys. Lett.* **6**, 279 (2009).

[12] M. Henke, J. Perßon, S. Kück, *J. Lumin.* **87-89**, 1049 (2000).

[13] M.A. Noginov, G.B. Loutts, D.E. Jones, V.J. Turney, R.R. Rachimov, L. Herbert, A. Truong, *J. Appl. Phys.* **91**, 569 (2002).

[14] G.B. Loutts, M. Warren, R. Taylor, R.R. Rachimov, H.R. Ries, G. Miller, M.A. Noginov, M. Curley, N. Noginova, N. Kuchtarev, H.J. Caulfield, P. Venkateswarlu, *Phys. Rev. B* **57**, 3706 (1998).

[15] J.A. Mares, M. Nikl, P. Maly, K. Bartos, K. Nejezchleb, K. Blezek, F. Noteristefani, C. D'Ambrossio, D. Puertolas, E. Rosso, *Opt. Mater.* **19**, 117 (2002).

[16] Yu. Zorenko, V. Gorbenko, I. Konstankevych, A. Voloshinovskii, G. Stryganyuk, V. Mikhailin, V. Kolobanov, D. Spassky, *J. Lumin.* **114**, 85 (2005).

[17] A. Yoshikawa, M. Nikl, G. Boulon, T. Fukuda, *Opt. Mater.* **30**, 6 (2007).

[18] S. Kobyakov, A. Kaminska, A. Suchocki, D. Galanciak, M. Malinowski, *Appl. Phys. Lett.* **88**, 234102 (2006).

[19] K.H. Young, D.D. Strother, *Physica C* **208**, 1 (1993).

[20] J.J. Robles, A. Bartasyte, H.P. Ng, A. Abrutis, F. Weiss, *Physica C* **400**, 36 (2003).

[21] Y. Konishi, M. Kasai, M. Izumi, M. Kawasaki, Y. Tokura, *Mater. Sci. Eng. B* **56**, 158 (1998).

[22] Y. Hu, M. Bator, M. Kenzelmann, T. Lippert, C. Niedermayer, C.W. Schneider, A. Wokaun, *Appl. Surf. Sci.* **258**, 9323 (2012).

[23] M. Jourdan, A. Zakharov, M. Foerster, H. Adrian, *J. Magn. Magn. Mater.* **272-276**, e163 (2004).

[24] P.H. Klein, W.J. Croft, *J. Appl. Phys.* **38**, 1603 (1967).

[25] J.D. Foster, L.M. Osterink, *Appl. Opt.* **7**, 2428 (1968).

[26] S. Geller, G.P. Espinosa, P.B. Crandall, *J. Appl. Crystallogr.* **2**, 86 (1969).

[27] R. Wynne, J.L. Daneu, T.Y. Fan, *Appl. Opt.* **38**, 3282 (1999).

[28] X. Xu, Zh. Zhao, H. Wang, P. Song, G. Zhou, J. Xu, P. Denga, *J. Cryst. Growth* **262**, 317 (2004).

[29] P. Goel, R. Mittal, N. Choudhury, S.L. Chaplot, *J. Phys., Condens. Matter* **22**, 065401 (2010).

[30] Z. Huang, J. Feng, W. Pan, *Solid State Commun.* **151**, 1559 (2011).

[31] D.D. Young, K.C. Jungling, T.L. Williamson, E.R. Nichols, *IEEE J. Quantum Electron.* **8**, 720 (1972).

[32] J. Ranløv, K. Nielsen, *J. Appl. Cryst.* **28**, 436 (1995).

[33] O. Chaix-Pluchery, B. Chenevier, J.J. Robles, *Appl. Phys. Lett.* **86**, 251911 (2005).

[34] L. Vasylechko, A. Senyshyn, U. Bismayer, in: *Handbook on the Physics and Chemistry of Rare Earths*, Vol. 39, Eds. K.A. Gschneidner, Jr., J.-C.G. Bünzli, V.K. Pecharsky, North-Holland, Netherlands 2009, p. 113.

[35] Y. Lu, Y. Dai, Y. Yang, J. Wang, A. Dong, B. Sun, *J. Alloys Comp.* **453**, 482 (2008).

[36] Q. Dong, G. Zhao, J. Chen, Y. Ding, Ch. Zhao, *J. Appl. Phys.* **108**, 023108 (2010).

[37] D.I. Savytski, L.O. Vasylechko, A.O. Matkovskii, I.M. Solskii, A. Suchocki, D.Yu. Sugak, F. Wallrafen, *J. Cryst. Growth* **209**, 874 (2000).

[38] M. Hoelzel, A. Senyshyn, N. Juenke, H. Boysen, W. Schmahl, H. Fuess, *Nucl. Instrum. Methods Phys. Res. A* **667**, 32 (2012).

[39] J. Rodrıguez-Carvajal, *Commiss. Powder Diffr. Newslett.* **26**, 12 (2001).

[40] L. Vočadlo, K.S. Knight, G.D. Price, I.G. Wood, *Phys. Chem. Miner.* **29**, 132 (2002).

[41] A. Senyshyn, D.M. Trots, J.M. Engel, L. Vasylechko, H. Ehrenberg, T. Hansen, M. Berkowski, H. Fuess, *J. Phys., Condens. Matter* **21**, 145405 (2009).

[42] D.M. Trots, A. Senyshyn, L. Vasylechko, R. Niewa, T. Vad, V.B. Mikhailik, H. Kraus, *J. Phys., Condens. Matter* **21**, 325402 (2009).

[43] A.M. Hofmeister, K.R. Campbell, *J. Appl. Phys.* **72**, 638 (1992).

[44] P.R. Stoddart, P.E. Ngoepe, P.M. Mjwara, J.D. Comins, G.A. Saunders, *J. Appl. Phys.* **73**, 7298 (1993).

[45] W.J. Alton, A.J. Barow, *J. Appl. Phys.* **32**, 1172 (1967).

[46] Y.-N. Xu, W.Y. Ching, *Phys. Rev. B* **59**, 10530 (1999).

[47] H. Buschmann, J. Dolle, S. Berendts, A. Kuhn, P. Bottke, M. Wilkening, P. Heitjans, A. Senyshyn, H. Ehrenberg, A. Lotnyk, V. Duppel, L. Kienle, J. Janek, *Phys. Chem. Chem. Phys.* **13**, 19378 (2011).

[48] A. Senyshyn, M. Hoelzel, T. Hansen, L. Vasylechko, V. Mikhailik, H. Kraus, H. Ehrenberg, *J. Appl. Crystallogr.* **44**, 319 (2011).

[49] D. Savytskii, L. Vasylechko, A. Senyshyn, A. Matkovskii, C. Bähtz, M.L. Sanjuán, U. Bismayer, M. Berkowski, *Phys. Rev. B* **68**, 024101 (2003).

[50] A.D. Fortes, I.G. Wood, L. Vočadlo, H.E.A. Brand, K.S. Knight, *J. Appl. Crystallogr.* **40**, 761 (2007).

[51] Ya. Zhydachevskii, D. Galanciak, S. Kobyakov, M. Berkowski, A. Kaminska, A. Suchocki, Ya. Zakharko, A. Durygin, *J. Phys., Condens. Matter* **18**, 11385 (2006).

[52] Xiang Wu, Shan Qin, Ziyu Wu, *J. Phys., Condens. Matter* **18**, 3907 (2006).

[53] N.L. Ross, J. Zhao, R.J. Angel, *J. Solid State Chem.* **177**, 1276 (2004).

[54] A. Senyshyn, A.R. Oganov, L. Vasylechko, H. Ehrenberg, U. Bismayer, M. Berkowski, A. Matkovskii, *J. Phys., Condens. Matter.* **16**, 253 (2004).

[55] A. Senyshyn, L. Vasylechko, M. Knapp, U. Bismayer, M. Berkowski, A. Matkovskii, *J. Alloys Comp.* **382**, 84 (2004).

[56] A. Senyshyn, H. Ehrenberg, L. Vasylechko, J.D. Gale, U. Bismayer, *J. Phys., Condens. Matter* **17**, 6217 (2005).

[57] A. Senyshyn, H. Boysen, R. Niewa, J. Banys, M. Kinka, Ya. Burak, V. Adamiv, F. Izumi, I. Chumak, H. Fuess, *J. Phys. D, Appl. Phys.* **45**, 175305 (2012).

[58] L. Vasylechko, A. Matkovski, A. Suchocki, D. Savytskii, I. Syvorotka, *J. Alloys Comp.* **286**, 213 (1999).

[59] L. Vasylechko, A. Matkovskii, D. Savytskii, A. Suchocki, F. Wallrafen, *J. Alloys Comp.* **292**, 57 (1999).

[60] L. Vasylechko, Ye. Pivak, A. Senyshyn, D. Savytskii, M. Berkowski, H. Borrmann, M. Knapp, C. Paulmann, *J. Solid State Chem.* **178**, 270 (2005).